Acta Mech 212, 167–179 (2010)
DOI 10.1007/s00707-009-0246-4

Jacob M. Wernik · Shaker A. Meguid

Atomistic-based continuum modeling of the nonlinear behavior of carbon nanotubes

Received: 6 August 2009 / Revised: 2 September 2009 / Published online: 11 November 2009

Abstract It is the purpose of this paper to determine the nonlinear mechanical properties of carbon nanotubes (CNTs). Due to the inherent nano-scale involved in simulating CNT structures, an atomistic description is incorporated via an atomistic-based continuum multiscale modeling technique. In this way, the continuum constitutive relations are derived solely from atomistic formulations. The atomic interactions in the CNT structure are described in a continuum framework using the Modified Morse interatomic potential. The effect of the angle-bending component of the potential is investigated and found to play a significant role in the stability of the structure. The nonlinear response of armchair and zigzag nanotubes under tensile and torsional loading conditions are considered and presented. In addition, the fracture process under tensile loading and the phenomena of torsional buckling are investigated.

1 Introduction

Since their discovery by Iijima [1], carbon nanotubes (CNTs) have been the subject of intense research; primarily because of their remarkable properties which include their miniature size, high aspect ratio, low density, high strength and high stiffness. The exceptional mechanical properties of CNTs have shown great promise for a wide variety of applications, such as nanotransistors, semiconductors, hydrogen storage devices, structural materials, molecular sensors, field-emission based displays, fuel cells, and as reinforcing agents in composite materials [2]. CNTs can generally be visualized as rolled sheets of graphene which are sometimes capped at each end. They exist in two forms, single-walled carbon nanotubes (SWCNT), which can have diameters as small as 0.4 nm, and multi-walled carbon nanotubes (MWCNTs), which exist as several SWCNTs embedded in one another with outside diameters in the range of 5–100 nm. A schematic illustration of an unrolled hexagonal graphene sheet is shown in Fig. 1. CNTs are defined by a pair of indices (n,m) which are used to identify their atomic structure and size. These indices correspond to a lattice vector $\mathbf{R} = n\mathbf{r}_1 + m\mathbf{r}_2$ on the graphene plane, where $\mathbf{r}_1$ and $\mathbf{r}_2$ are unit vectors in the hexagonal lattice, and n and m are integers. Two main CNT symmetry groups exist: the armchair (n,n) configuration, and the zigzag (n,0) configuration, with all other (n,m) combinations referred to as chiral nanotubes. The CNT radius and chiral angle can be determined from the following expressions:

J. M. Wernik · S. A. Meguid (✉)
Engineering Mechanics and Aerospace Design Laboratory, Department of Mechanical and Industrial Engineering, University of Toronto, 5 King's College Road, Toronto, ON M5S 3G8, Canada
E-mail: meguid@mie.utoronto.ca
Tel.: +1-416-9785741
Fax: +1-416-9787753

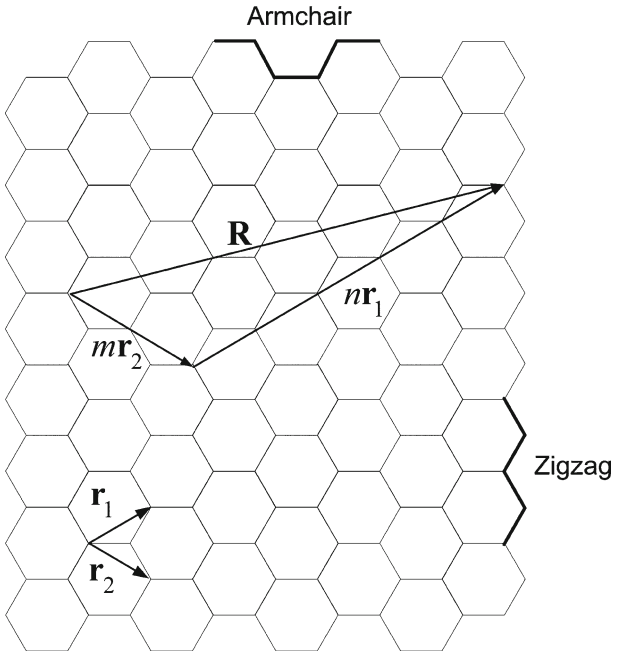

Fig. 1 Chiral vector definition

$$r_{\mathrm{CNT}} = \frac{\sqrt{3} r_o}{2\pi} \sqrt{n^2 + mn + m^2}, \tag{1}$$

$$\theta = \cos^{-1} \frac{2n + m}{2\sqrt{n^2 + mn + m^2}}, \tag{2}$$

where r_o is the equilibrium carbon–carbon (C–C) covalent bond length normally taken to be 0.1421 nm.

The use of CNTs in structural applications requires a thorough understanding of their mechanical properties and fracture processes under a variety of different loading conditions. In the above applications both tensile and torsional loads can occur on the CNTs. Therefore, in order to optimize the design of CNT devices, a detailed understanding of the mechanical response of CNTs under both tensile and torsional loads is required.

To date, a number of researchers have employed both experimental and theoretical techniques to characterize the mechanical properties of CNTs. However, due to the extremely small size of CNTs, the experimental studies are extremely challenging and their measurements are fairly limited [3,4]. According to the experimental measurements of Yu et al. [3], the tensile strengths of MWCNTs can range from 11 to 63 GPa while the Young's modulus ranges from 270 to 950 GPa. They also observed that the MWCNTs broke in the outermost layer giving rise to a 'sword-in-sheath' failure mechanism. On the other hand, the theoretical approaches to characterizing the mechanical properties and failure mechanisms of CNTs are numerous. Researchers have used modeling methods from all length scales to characterize the behavior of CNTs. First principle quantum mechanical descriptions have been employed to model the structural deformation [5], fracture [6], defect nucleation [7], chemical reactivity [8,9], and fuctionalization [10,11] of individual CNTs. Classical molecular dynamic and molecular mechanic simulations have been shown to play an important role in determining the constitutive relations of CNTs under different loading conditions [12–14], CNT growth mechanisms [15], oscillatory properties [16], and the effects of chirality and length on the mechanical properties [17]. At the coarser end of the length scale, continuum mechanical concepts have also been used in characterizing CNT behavior. CNTs behave much like slender hollow cylinders under bending and compression and seem to display continuum characteristics such as a constitutive behavior similar to Hooke's law. In continuum-based approaches the CNT is modeled as a continuous shell with a fixed wall thickness and material properties [18–20]. However, the only way of distinguishing between nanotubes of different chirality (zigzag, armchair, chiral) is through the radius of the shell. The disadvantages of this approach are that the CNT is drastically

oversimplified, it cannot be used to study the effect of defects, and the atomic structure of the CNT has been ignored.

Traditional continuum mechanics models cannot accurately describe the mechanical properties of CNT structures because they lack the atomistic representation and appropriate constitutive relations that govern material behavior at this scale. At the nano-scale, traditional continuum mechanical concepts do not maintain their validity [21] and gross oversimplifications can arise from the use of a purely continuum model. Full atomistic descriptions are also unrealistic. They are computationally intensive and are limited by the realistic system sizes that they can represent due to the enormous number of degrees of freedom involved. Even the use of state-of-the-art parallel supercomputers can only handle a limited number of atoms ($\sim 10^9$), corresponding to less than one cubic micron [22,23]. Since various scales in the system depend on each other, it is necessary to formulate it in terms of multiscale modeling.

In this study, the atomistic-based continuum multiscale modeling technique is used to predict the mechanical behavior of CNTs. It has the unique advantage of describing the atomic-property relations of the structure in a continuum framework. In this case, the continuum constitutive models are derived purely from atomistic principles. The deformation measures introduced in the model capture the underlying atomistic structure of the different phases considered. As a result, the significance of these measures is fundamentally different from those in the classical continuum theory. For example, in the case of CNT systems, it is important to consider the atomic bonding and interaction between the carbon atoms in the CNT lattice. This is typically carried out at the atomistic scale using appropriate interatomic potentials. This leads to an atomistic constitutive law between the force and the displacement. The strength of atomistic-based continuum techniques lies in their ability to avoid the large number of degrees of freedom typically encountered in coupled atomistic discrete modeling techniques.

In the development of a computational model for the study of CNT structures it is necessary to consider the integration of atomistic and continuum scales, and the nonlinearity of the atomic interactions. It is important to include an atomistic description in the form of interatomic potentials because they provide the constitutive relations for these classes of materials at the atomistic scale. They describe how the atomic interactions behave under different loading conditions and atomic environments. The general form of an interatomic potential, or equivalently, the energy of a molecule is given by:

$$E_{\text{tot}} = E_{\text{bonded}} + E_{\text{non-bonded}}. \tag{3}$$

The bonded interactions can be further subdivided as

$$E_{\text{bonded}} = E_s + E_b + E_t + E_I, \tag{4}$$

where E_s, E_b, E_t and E_I correspond to bond stretching, bond angle-bending, torsion and inversion energies, respectively. The non-bonded interactions can also be subdivided such that

$$E_{\text{non-bonded}} = E_{\text{vdW}} + E_{\text{es}} + E_{\text{hb}}, \tag{5}$$

where E_{vdW}, E_{es} and E_{hb} correspond to van der Waals forces, electrostatic forces and hydrogen bonding, respectively. The atomic bond deformation mechanisms are depicted in Fig. 2; excluding the electrostatic and hydrogen bonding forces. Interatomic potentials are nonlinear in nature. Therefore, in order to provide a realistic description of the system, the nonlinearity of the potentials must be considered in any simulation. It is with the above in mind that an atomistic-based continuum model is proposed to investigate the nonlinear mechanical behavior of CNTs. The mechanical properties of the CNTs structures are explored under both tensile and torsional loading conditions.

2 Atomistic-based continuum model

In this study, two distinct CNT structures were investigated: the (16,0) zigzag nanotube and the (9,9) armchair nanotube, each having an approximate diameter of 1.2 nm. The CNT was modeled as a space-frame structure as depicted in Fig. 3. The figure also illustrates a portion of the hexagonal lattice to demonstrate that beam elements were used in the representation of the individual C–C covalent bonds in the FE framework. As in traditional FE models, nodes were used to connect the beam elements to form the CNT structure. In this case the nodes represent the carbon atoms and are defined by the same atomic coordinates. The Modified Morse interatomic potential was used to describe the behavior of the atomic interactions in the CNT. This potential

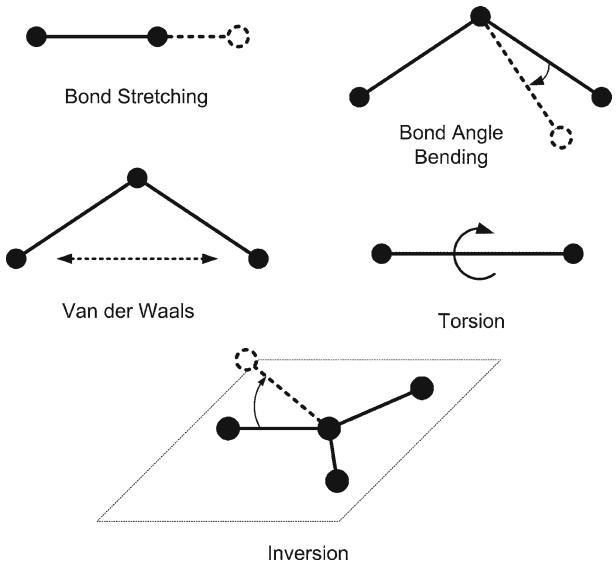

Fig. 2 Atomic bond deformation mechanisms

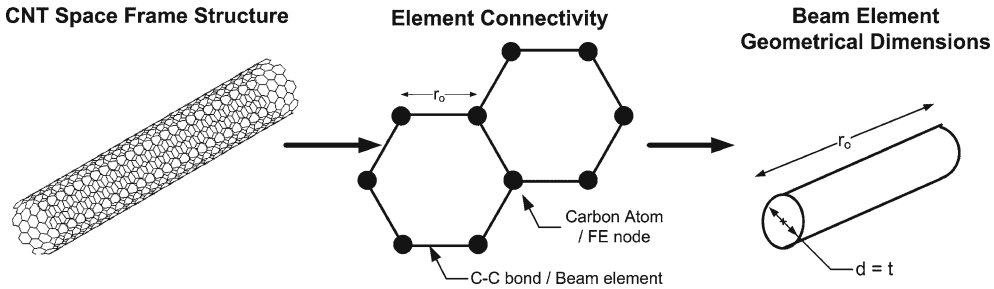

Fig. 3 The carbon nanotube space frame structure

is well suited for characterizing the behavior of C–C covalent bonding, and has been used by several authors in both purely atomistic [15,24] and atomistic-based continuum simulations [25–28] of CNT fracture and growth. This potential consists of two parts: a bond stretching component and an angle-bending component, as given by:

$$E = E_s + E_b, \tag{6}$$

$$E_s = D_e \left(\left[1 - \exp^{-\beta(r - ro)} \right]^2 - 1 \right), \tag{7}$$

$$E_b = \frac{1}{2} k_\theta \left(\theta - \theta_o \right)^2 \left[1 + k_{\text{sextic}} \left(\theta - \theta_o \right)^4 \right], \tag{8}$$

where r is the current bond length, θ is the current angle of the adjacent bond, D_e is the dissociation energy, and β is a constant which controls the 'width' of the potential. The parameters used for the potential in this study were the same as those adopted by Belytschko et al. [24], and are presented in Table 1. This is the usual form of the Morse potential except that the angle-bending component has been added and the parameters are slightly modified to correspond with the Brenner potential for strains below 10%. The reason for this being that the Brenner potential is considered more accurate and versatile due to its ability to account for bond hybridization and bonds with atoms other than carbon. Tserpes et al. [29] suggest that the angle-bending component can be neglected. However, this component has been found to contribute to the initial stability of the CNT. Without the addition of the angle-bending component, the CNT will experience unstable configuration and tends to collapse on itself.

In this paper, nonlinear rotational spring elements were used to account for the angle-bending component, while beam elements were used to represent the stretching component of the potential. In order to

Table 1 Modified Morse potential parameters

Parameter	Value	Parameter	Value
r_o(m)	1.421×10^{-10}	θ_o(rad)	2.094
D_e(N m)	6.03105×10^{-19}	k_θ(N m rad^{-2})	0.876×10^{-18}
B(m^{-1})	2.625×10^{10}	k_{sextic}(rad^{-4})	0.754

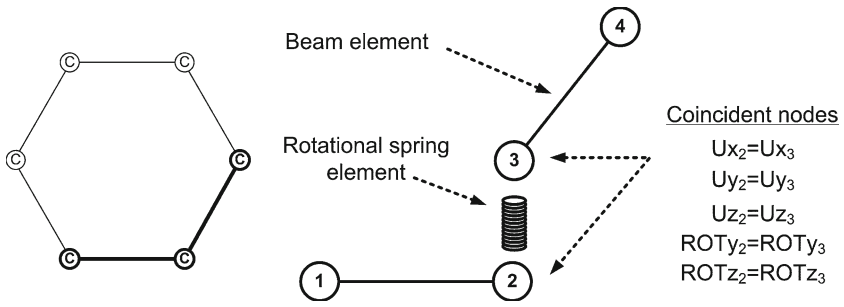

Fig. 4 Coincident node locations in defining the rotational spring element

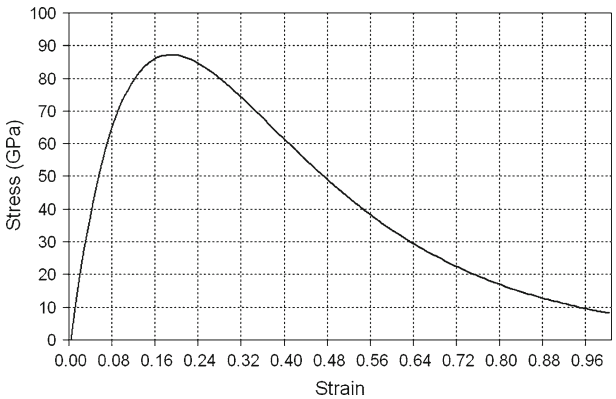

Fig. 5 The stress–strain relationship for the beam elements as derived from the Modified Morse potential

ensure an appropriate connectivity and transmission of moments among adjacent beam elements, the rotational springs were defined between coincident nodes with coupled translational and rotational degrees of freedom, as depicted in Fig. 4. To describe the behavior of the beam and rotational spring elements, we first derive material models for each which accurately represents the characteristics of the Modified Morse potential. First, by deriving the stretching potential (Eq. 7) with respect to the change in bond length and by utilizing the following relationship, $\varepsilon = (r - r_o)/r$, we can arrive at the expression:

$$F = 2\beta D_e \left(1 - \exp^{-\beta\varepsilon r}\right) \exp^{-\beta\varepsilon r}, \tag{9}$$

which represents the force required to stretch a C–C bond. The interlayer spacing of CNT walls was assumed to be 0.34 nm and is also widely regarded as the CNT wall thickness [30–33]. This implies that the diameter of each bond or beam element is also 0.34 nm. The corresponding cross-sectional area is 0.09079 nm^2. Utilizing this area and the above expression in Eq. (9), we were able to derive the stress–strain relationship (Fig. 5) for the beam elements. This relationship was used to describe the behavior of the beam elements up to a critical strain of 19% at which point the stiffness of the beams approaches zero and the bond has essentially been broken. The initial stiffness of the beam elements was calculated to be 1.3 TPa.

Similarly, recognizing that the derivative of the angle-bending component of the potential with respect to the change in rotation is equivalent to the moment required to bend neighboring bonds, we can arrive at the following expression:

$$M = k_\theta \Delta\theta \left[1 + 3k_{\text{sextic}} (\Delta\theta)^4\right]. \tag{10}$$

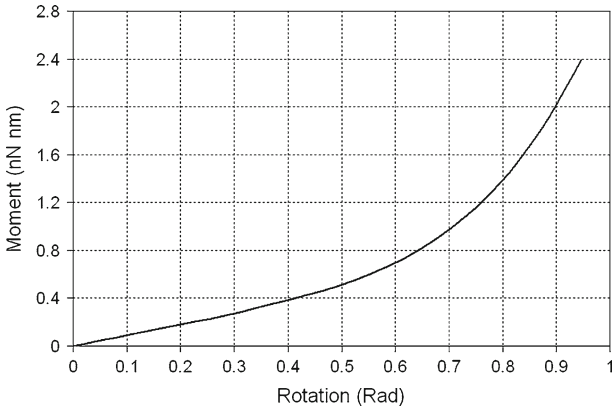

Fig. 6 Moment/rotation curve for the angle bending component of the Modified Morse potential

The moment/rotation curve obtained from Eq. (10) is shown in Fig. 6. Again, this curve was used to define the stiffness of the rotational spring elements throughout the simulation. The initial stiffness was calculated to be 8.76×10^{-10} N nm rad^{-2}.

Given the appropriate set of interatomic potentials and corresponding parameters, the other bond deformation mechanisms can also be included, i.e. dihedral angle torsion, out-of-plane torsion, van der Waals interactions and electrostatic interactions. However, several authors [30,34,35] have stated that these effects are negligible and play an insignificant role in the simulation of CNT structures.

3 Results and discussion

The nonlinear response of the individual CNTs was investigated. Two CNT arrangements were studied: the (16,0) zigzag nanotube and the (9,9) armchair nanotube, both having diameters of approximately 1.2 nm. Tensile and torsional loading conditions are investigated to obtain tensile and shear properties. In both cases, one end of the nanotube was completely restrained, while the other end was assigned a prescribed displacement. In computation, a pristine nanotube does not present a favorable location for fracture to nucleate due to the intrinsic symmetry of the defect-free nanotube structure. Instead, fracture will often nucleate simultaneously at multiple locations along the length of the tube. However, when the nanotube end is imposed with a rigid boundary constraint, stress concentrations near the constrained end are inevitable. Such an effect is likely to cause the bond lengths and bond angles near the tube ends to be different than the remaining part of the CNT. This will cause the nanotube to fail at the restrained end which is unrepresentative of the realistic failure process. In order for the nanotubes to fail elsewhere along their length, a defect must be introduced in the graphene lattice. In this study, a 5% weakening of a bond located halfway along the CNT length is introduced to initiate fracture in the desired location. A CNT length of 7 nm was determined to be sufficient in avoiding the effects of the constrained boundary conditions.

In typical atomic level simulations, the force acting in a structure is a more meaningful measure than the stress. However, in order to present the results in a universally recognized form and for the sake of comparison, it was decided to derive the uniaxial stress and plot it against the applied strain, ε, computed by $\varepsilon = (L - L_o)/L_o$, where L is the deformed length and L_o is the initial length of the nanotube. To do so, a corresponding area must be defined. Here, the cross-sectional area is defined as $A_o = \pi Dt$, where D is the diameter of the nanotube and t is the thickness taken to be equal to 0.34 nm. Therefore, we can define the uniaxial stress acting in the nanotube as

$$\sigma = \frac{F_\sigma}{A_o} = \frac{F_\sigma}{\pi Dt}, \tag{11}$$

where the total axial force, F_σ, is obtained by summing the interatomic forces acting on the atoms at the restrained end of the CNT.

The predicted tensile stress–strain curves for both armchair and zigzag CNT arrangements are presented in Fig. 7, while the corresponding mechanical properties are provided in Table 2. From the stress–strain curves, we can see that the zigzag nanotube can withstand a strain of 17.5%, while the armchair nanotube can withstand

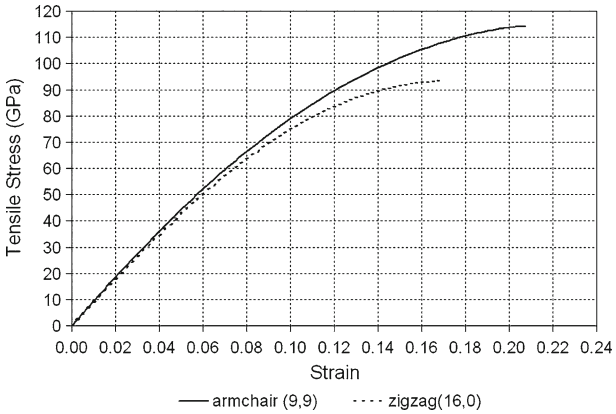

Fig. 7 Carbon nanotube stress–strain curves

Table 2 Tensile properties of armchair and zigzag carbon nanotubes

Property	Zigzag (16,0)	Armchair (9,9)
Tensile modulus (GPa)	920.2	944.8
Maximum tensile stress (GPa)	93.4	114.4
Maximum tensile strain (%)	17.5	20.7

Table 3 Comparison of tensile and shear moduli with other corresponding results available in literature

	E (TPa)	G (TPa)
Theoretical models		
Present study	0.9202/0.9448	0.3442/0.3434
Giannopoulos et al. [36]	1.2478	0.3245
Lu [31]	0.9727	0.4550
Hernandez et al. [32]	1.2400	–
Srivastava and Wei [37]	0.9000	0.3000
Li and Chou [30]	0.9947	0.3921
Gupta et al. [38]	1.2238	0.3281
Jin and Yuan [33]	1.2360	0.4920
Tserpes and Papanikos [29]	1.0293	0.4330
To [39]	1.0300	0.4750
Shen and Li [40]	1.2000[a]	0.5000[a]
Experimental methods		
Krishman et al. [41]	1.3000	–
Yu et al. [3]	1.0200	–
Tombler et al. [42]	1.2000	–
Hall et al. [43]	–	0.4100

[a] As deduced from Figs. 3b and 6b in [40]

a strain of up to 20.7%. The respective tensile modulus for the armchair and zigzag nanotubes are 944.8 and 920.2 GPa. A comparison with other reported tensile moduli is shown in Table 3. The overall trend of the stress–strain curves agrees well with others in the literature [24,27,29,44], and also shows that the armchair configuration exhibits higher strength and stiffness when compared to the zigzag configuration. Figure 7 leads us to deduce that given the appropriate bonding, dispersion, and alignment, the armchair nanotube will act as a better reinforcing agent in composite materials, when compared to the zigzag configuration.

It should be noted that the Modified Morse potential is not appropriate for describing the behavior of CNTs after bonds are broken since it does not consider the formation of new bonds and the possibility that rehybridization and structural transformations may occur. However, it has been shown that the fracture strength of CNTs depends primarily on the inflection point of the potential [24]. Therefore, since the inflection strain occurs well before the strain required to break bonds and form new ones, we are provided with some confidence that the Modified Morse potential can give a correct picture of the tensile properties of CNTs up to failure.

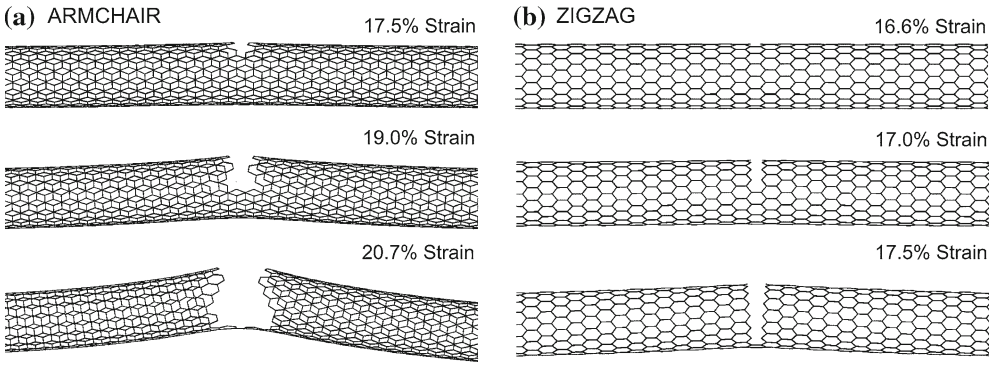

Fig. 8 Nanotube fracture processes under tensile loading for **a** armchair and **b** zigzag configurations

Also, from both experimental [3] and theoretical studies it has been determined that the stress suddenly drops to zero once the maximum tensile strength has been reached. Therefore, the reported maximum stresses and strains corresponding to the inflection point on the stress–strain curves are taken as the tensile capacity of the nanotube.

Of interest to the present study are the deformation mechanisms of CNTs under both tensile and torsion loading conditions. Figure 8a and b show the tensile fracture process for both armchair and zigzag nanotubes, respectively. For both cases the nanotubes simply elongate with little reduction in their cross-sectional area until they fracture. Fracture initiates at the weakened bond. For the case of the armchair nanotube, fracture occurs gradually. At 17.4% strain the first bonds are broken which leads to the successive elongation and failure of neighboring bonds. At a critical strain of 20.7% all the bonds along the circumference of the nanotube have broken. In this case, the bonds fail in an irregular pattern and give rise to a large hole on the surface of the CNT. For the case of the zigzag nanotube fracture occurs almost instantaneously. At a strain of 16.6% the weakened bond has reached its critical strain and breaks, which causes the adjacent bonds along the circumference of the nanotube to take up the load. At a strain of 17.5% nearly all the adjacent bonds have broken and the zigzag nanotube has fractured. From this we can conclude that the zigzag nanotube exhibits brittle behavior at fracture. Also, the fracture process resembles the propagation of an ideal crack through the nanotube in a direction orthogonal to the nanotube longitudinal axis.

We can attribute the differences in strength, strain at fracture, and the fracture processes to the orientation of the bonds in the nanotube structures. For the case of the zigzag nanotube a large percentage of the bonds are orientated parallel to the axial loading direction. Thus, these bonds tend to carry most of the load and subsequently undergo larger elongations. In the case of the armchair nanotube, most of the bonds are orientated at a 30° angle to the loading direction. This causes the bonds to fail in an irregular pattern at larger strains. Figure 9 plots the elongation of the weakened bonds in both structures against the axial strain of the nanotube. The results are only extended to a critical bond elongation of 0.027 nm which corresponds to the 19% inflection strain of the Modified Morse potential. The figure clearly confirms that the bond in the zigzag nanotube reaches its critical elongation at lower axial nanotube strain values when compared to the armchair nanotube. The tensile fracture process for both armchair and zigzag configurations are in agreement with those of Belytschko et al. [24], Lu and Bhattacharya [45], and Meo and Rossi [44].

The CNT was simulated with a diminishing rotational spring element stiffness to demonstrate the effect of omitting the angle bending component of the Modified Morse potential. The corresponding stress–strain curve is provided in Fig. 10. As can be seen, the CNT provided no response to the initial loading. This can be attributed to the fact that the bending of adjacent bonds is responsible for the initial deformation of the CNT. The initial elastic stretching of a nanotube occurs due to the elongation of the hexagons in the nanotube wall by way of adjacent bonds bending relative to each other and not by the stretching of the individual bonds themselves. Without the angle bending component of the Modified Morse potential the CNT tends to collapse on itself or slacks, as depicted in Fig. 11 for the case of the zigzag nanotube, until enough loading has been applied to stiffen the structure. However, apart from this initial stiffening effect, the angle-bending component contributes insignificantly to the overall fracture behavior of the CNT. Therefore, it can be concluded that the bond angle bending component of the Modified Morse potential is essential in establishing an equilibrium

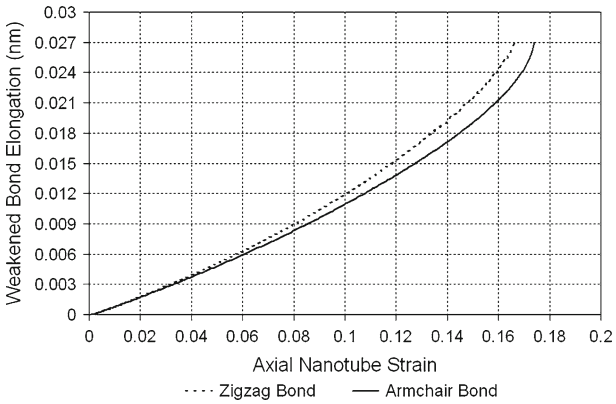

Fig. 9 Elongations of weakened bonds plotted against the axial strain of the nanotube

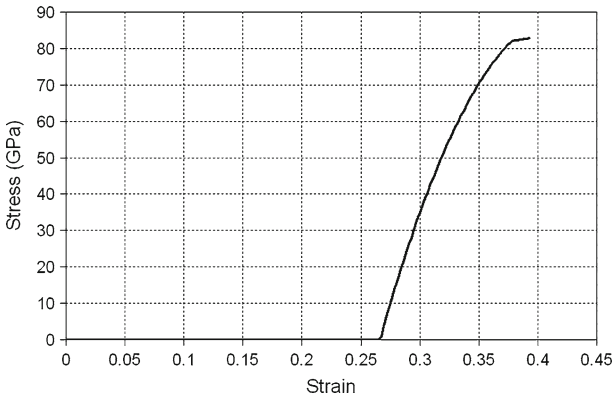

Fig. 10 Effect of omitting the bond-angle bending component of the Modified Morse potential on the tensile stress strain curve

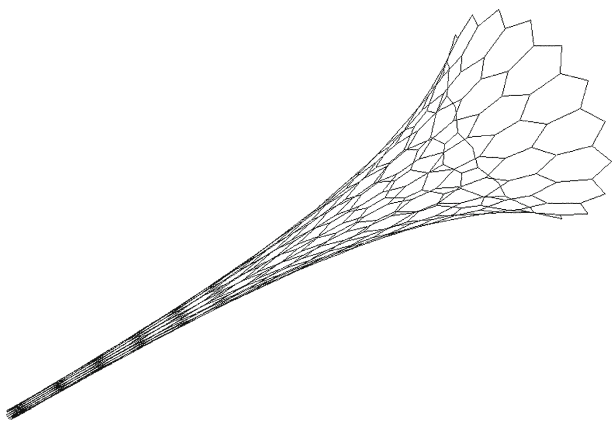

Fig. 11 Collapsed CNT structure due to omitting the bond-angle bending component of the Modified Morse potential

configuration of the nanotube but plays no role in the fracture process. The same behavior has been observed by Belytschko et al. [24] in their atomistic simulations of nanotube fracture.

As in the case of the tensile loading scenario it is also useful to define the shear stress due to torsion so that the results may be presented in a recognized form. Here, the shear stress is defined in a similar manner to the above uniaxial stress ($\tau = F_\tau / A_o$) where the cross sectional area also remains the same, however, the total shear force, F_τ, is now computed by summing the reaction forces acting in the tangential direction of all the atoms at the restrained end of the nanotube. The shear strain is defined as $\gamma = r\Delta\theta / L_o$, where r is the radius of the nanotube, $\Delta\theta$ is the rotation of the nanotube around the z-axis, and L_o is the initial length of the

Table 4 Shear properties of armchair and zigzag carbon nanotubes

Property	Zigzag (16,0)	Armchair (9,9)
Shear modulus (GPa)	344.2	343.4
Maximum shear stress (GPa)	111.1	105.5
Maximum shear strain (%)	37.0	38.0

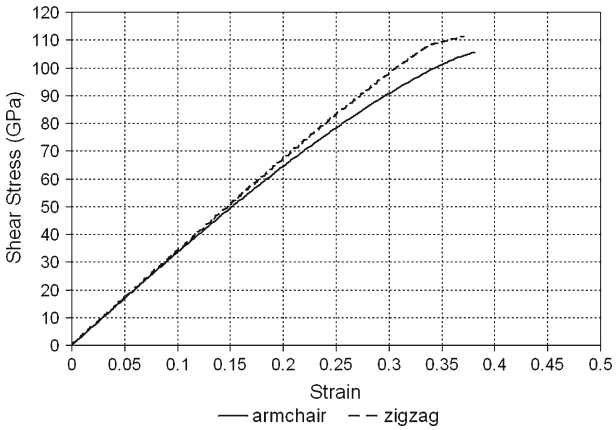

Fig. 12 Carbon nanotube shear stress–shear–strain curves

nanotube. The shear loads were induced by applying a prescribed tangential displacement at the free end of the nanotube while restraining the axial and radial displacements.

The shear stress–strain curves for both nanotubes are shown in Fig. 12 along with the corresponding properties of relevance in Table 4. The shear modulus for zigzag and armchair nanotubes was 344.2 and 343.4 GPa, respectively. Shown in Table 3, these values do agree with several quoted values in literature [36–38]. For example, Giannopoulos et al. [36] developed a nanotube model using a spring-based finite element approach. They used simple harmonic potentials to derive the stiffness of the elements in their model. However, instead of using beam elements, Giannopoulos et al. used truss rods to model individual C–C bonds as well as the bond-angle bending component of the potential. The average value over a sample size of ten different chiralities was given as 324.5 GPa. The shear stress–strain curves also show good overall agreement with those presented by Xiao et al. [46]. In their paper, the predicted shear strength for both armchair and zigzag nanotubes was 108 GPa with corresponding failure strains in the range of 27–33%. In comparison, the present study has predicted shear strengths of 105 and 111 GPa for armchair and zigzag nanotubes, respectively, with corresponding failure strains of approximately 38–37%. From Fig. 12 it can also be concluded that the shear stress–strain relationships are approximately linear up to their critical values which indicate that the shear modulus is insensitive to the strain.

Figure 13a and b show the torsional deformation process for both armchair and zigzag nanotubes, respectively. In torsion, the nanotubes first twist with little or no change in their cylindrical geometry until an approximate shear strain of 15 and 25% for armchair and zigzag nanotubes, respectively. At this shear strain, the nanotubes begin to show localized collapse or the onset of torsional buckling. It is also at these corresponding strains that the shear stress–strain curves begin to deviate from their initial linear behavior. These shear strains correspond to an angle of twist equal to 1.33 and 2.09 rad for armchair and zigzag nanotubes, respectively. Therefore, it is probable that nanotubes with a zigzag structure possess higher resistance to torsional buckling than the armchair nanotubes. At respective critical shear strains of approximately 38 and 37%, the armchair and zigzag nanotubes have collapsed entirely in the localized zone and take the form of straight axis spirals. At the critical strains nearly all the bonds along the periphery of the spiral have been broken as illustrated in Fig. 14 for the case of the armchair nanotube where the broken bonds are highlighted in white. The observed torsional deformation processes are consistent with those observed both theoretically by means of molecular dynamics simulations by Yakobson et al. [47] and experimentally by Yu et al. [48].

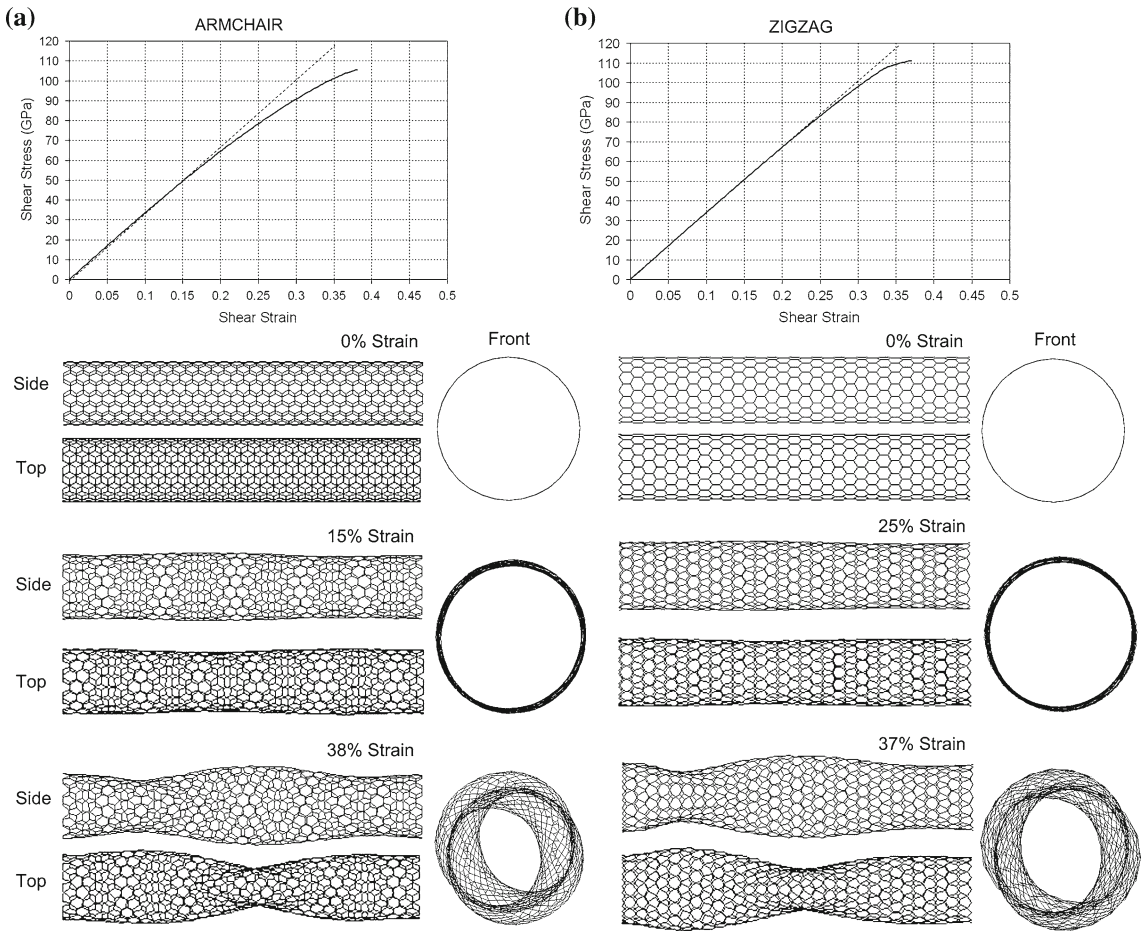

Fig. 13 Nanotube deformation processes under torsional loading for **a** armchair and **b** zigzag configurations

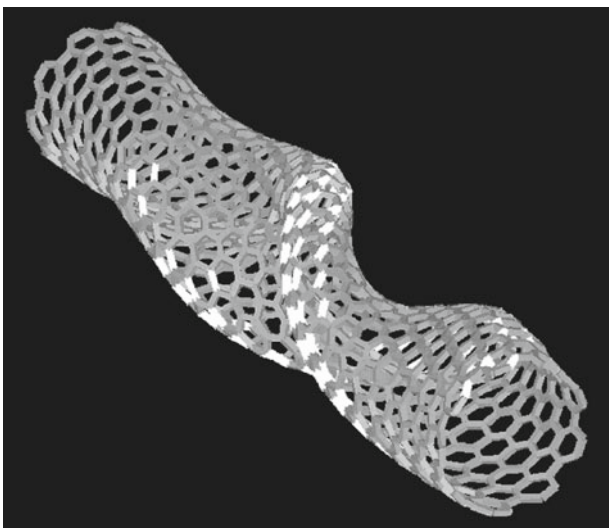

Fig. 14 The armchair nanotube after collapse under torsional loading. The white elements along the periphery of the spiral indicate the bonds that have broken

4 Conclusions

A nonlinear atomistic-based continuum model has been developed for the study of CNT structures. An atomistic description has been incorporated through the integration of the Modified Morse potential. The nonlinear mechanical properties of both zigzag and armchair nanotubes have been presented. From the predicted results the following conclusions can be drawn:

(i) The use of the Modified Morse potential to describe the behavior of carbon–carbon bonding in the CNT can reasonably predict the nonlinear response of both armchair and zigzag nanotubes under both tensile and torsional loads.
(ii) The angle-bending component of the Modified Morse potential is responsible for the initial stability of the CNT.
(iii) Given the appropriate bonding, dispersion, and alignment, the armchair nanotube will act as a better reinforcing agent in composite materials.
(iv) When introduced with a 5% weakened bond, fracture occurs gradually over a range of 3.3% strain for the case of the armchair nanotube. For the case of the zigzag nanotube, fracture occurs rapidly (less than 1%) and resembles the propagation of an ideal crack through the nanotube in a direction orthogonal to the nanotube longitudinal axis.
(v) The shear properties for both nanotube configurations are very similar. In addition, both configurations also undergo torsional buckling. However, this phenomenon seems to occur at a lower angle of twist for the case of the armchair nanotube. Therefore, from the predicted results, the zigzag nanotube structure possesses a higher resistance to torsional buckling.

Acknowledgments The authors wish to acknowledge the financial support provided by the Natural Sciences and Engineering Research Council (NSERC) of Canada.

References

1. Iijima, S.: Helical microtubules of graphitic carbon. Nature **354**, 56–58 (1991)
2. Endo, M., Hayashi, T., Kim, Y.A., Terrones, M., Dresselhaus, M.S.: Applications of carbon nanotubes in the twenty-first century. Phil. Trans. R. Soc. Lond. A **362**, 2223–2238 (2004)
3. Yu, M.F., Lourie, O., Dyer, M.J., Moloni, K., Kelly, T.F., Ruoff, R.S.: Strength and breaking mechanism of multiwalled carbon nanotubes under tensile load. Science **287**, 637–640 (2000)
4. Demczyk, B.G., Wang, Y.M., Cumings, J., Hetman, M., Han, W., Zettl, A., Ritchie, R.O.: Direct mechanical measurement of the tensile strength and elastic modulus of multiwalled carbon nanotubes. Mater. Sci. Eng. A **334**, 173–718 (2002)
5. Chandraseker, K., Mukherjee, S.: Atomistic-continuum and ab initio estimation of the elastic moduli of single-walled carbon nanotubes. Comput. Mater. Sci. **40**, 147–158 (2007)
6. Troya, D., Mielke, S.L., Schatz, G.C.: Carbon nanotube fracture—differences between quantum mechanical mechanisms and those of empirical potentials. Chem. Phys. Lett. **382**, 133–141 (2003)
7. Ding, F.: Theoretical study of the stability of defects in single-walled carbon nanotubes as a function of their distance from the nanotube end. Phys. Rev. B **72**, 245409-1-7 (2005)
8. An, W., Wu, X., Yang, J.L., Zeng, X.C.: Adsorption and surface reactivity on single-walled boron nitride nanotubes containing stone-wales defects. J. Phys. Chem. C **111**, 14105–14112 (2007)
9. Galano, A., Francisco-Marquez, M.: Reactivity of silicon and germanium doped CNTs toward aromatic sulfur compounds: a theoretical approach. Chem. Phys. **345**, 87–94 (2008)
10. Zhao, J., Ding, Y.: Silicon carbide nanotubes functionalized by transition metal atoms: a density-functional study. J. Phys. Chem. C **112**, 2558–2564 (2008)
11. Wang, C., Zhou, G., Liu, H., Wu, J., Qiu, Y., Gu, B., Duan, W.: Chemical functionalisation of carbon nanotubes by carboxyl groups on stone-wales defects: a density functional theory study. J. Phys. Chem. B **110**, 10266–10271 (2006)
12. Cao, G., Chen, X.: Buckling behavior of single-walled carbon nanotubes and a targeted molecular mechanics approach. Phys. Rev. B **74**, 165422-1-10 (2006)
13. Gong, N., Liang, Y., Yao, Y., Liu, B.: Static and dynamic analysis of carbon nanotube cantilever based on molecular dynamics simulation. Key Eng. Mater. 375–376, 631–635 (2008)
14. Buehler, M., Kong, Y., Gao, H.: Deformation mechanisms of very long single-wall carbon nanotubes subject to compressive loading. J. Eng. Mater. Technol. **126**, 245–249 (2004)
15. Esfarjani, K., Gorjizadeh, N., Nasrollahi, Z.: Molecular dynamics of single wall carbon nanotube growth on nickel surface. Comput. Mater. Sci. **36**, 117–120 (2006)
16. Zhao, X., Cummings, P.T.: Molecular dynamics study of carbon nanotube oscillators revisited. J. Chem. Phys. **124**, 134705-1-8 (2006)
17. Cao, G., Chen, X.: The effects of chirality and boundary conditions on the mechanical properties of single-walled carbon nanotubes. Int. J. Solids Struct. **44**, 5447–5465 (2007)
18. Cao, G., Chen, X.: Buckling of single-walled carbon nanotubes upon bending: molecular dynamics simulations and the finite element method. Phys. Rev. B **73**, 155435-1-10 (2006)

19. Yakobson, B.I., Brabec, C.J., Bernhole, J.: Nanomechanics of carbon tubes: instabilities beyond linear response. Phys. Rev. Lett. **76**, 2511–2514 (1996)
20. Pantano, A., Parks, D.M., Boyce, M.C.: Mechanics of deformation of single- and multi-wall carbon nanotubes. J. Mech. Phys. Solids **52**, 789–821 (2004)
21. Chang, T., Geng, J., Guo, X.: Prediction of chirality- and size-dependent elastic properties of single-walled carbon nanotubes via a molecular mechanics model. Proc. R. Soc. A **462**, 2523–2540 (2006)
22. Rudd, R.E.: The atomic limit of finite element modeling in MEMS: Coupling of length scales. Analog Integr. Circuits Signal Process. **29**, 17–26 (2001)
23. Abraham, F.F., Walkup, R., Gao, H., Duchaineau, M., DeLa Rubia, T.D., Seager, M.: Simulating materials failure by using up to one billion atoms and the world's fastest computer: brittle fracture. Proc. Natl. Acad. Sci. USA **99**, 5777–5782 (2002)
24. Belytschko, T., Xiao, S.P., Schatz, G.C., Ruoff, R.S.: Atomistic simulations of nanotube fracture. Phys. Rev. B **65**, 1–8 (2002)
25. Liew, K.M., Chen, B.J., Xiao, Z.M.: Analysis of fracture nucleation in carbon nanotubes through atomistic-based continuum theory. Phys. Rev. B **71**, 235424-1-7 (2005)
26. Sun, X., Zhao, W.: Prediction of stiffness and strength of single-walled carbon nanotubes by molecular mechanics based finite element approach. Mater. Sci. Eng. A **390**, 366–371 (2005)
27. Xiao, J.R., Staniszewski, J., Gillespie, J.W. Jr.: Fracture and progressive failure of defective graphene sheets and carbon nanotubes. Compos. Struct. **88**, 602–609 (2009)
28. Natsuki, T., Endo, M.: Structural dependence of nonlinear elastic properties for carbon nanotubes using continuum analysis. Appl. Phys. A **80**, 1463–1468 (2005)
29. Tserpes, K.I., Papanikos, P., Labeas, G., Pantelakis, S.G.: Multi-scale modeling of tensile behavior of carbon nanotube-reinforced composites. Theor. Appl. Frac. Mech. **49**, 51–60 (2008)
30. Li, C., Chou, T.: A structural mechanics approach for the analysis of carbon nanotubes. Int. J. Solids Struct. **40**, 2487–2499 (2003)
31. Lu, J.P.: Elastic properties of carbon nanotubes and nanoropes. Phys. Rev. Lett. **79**, 1297–1300 (1997)
32. Hernandez, E., Goze, C., Bernier, P., Rubio, A.: Elastic properties of C and BxCyNz composite nanotubes. Phys. Rev. Lett. **80**, 4502–4505 (1998)
33. Jin, Y., Yuan, F.G.: Simulation of elastic properties of single-walled carbon nanotubes. Compos. Sci. Technol. **63**, 1507–1515 (2003)
34. Odegard, G.M., Gates, T.S., Nicholson, L.M., Wise, K.E.: Equivalent-continuum modeling of nano-structured materials. Compos. Sci. Technol. **62**, 1869–1880 (2002)
35. Natsuki, T., Tantrakan, K., Endo, M.: Effects of carbon nanotubes structures on mechanical properties. Appl. Phys. A **79**, 117–124 (2004)
36. Giannopoulos, G.I., Kakavas, P.A., Anifantis, N.K.: Evaluation of the effective mechanical properties of single walled carbon nanotubes using a spring based finite element approach. Comput. Mater. Sci. **41**, 561–569 (2008)
37. Srivastava, D., Wei, C.: Nanomechanics of carbon nanotubes and composites. Appl. Mech. Rev. **56**, 215–230 (2003)
38. Gupta, S., Dharamvir, K., Jindal, V.K.: Elastic moduli of single-walled carbon nanotubes and their ropes. Phys. Rev. B **72**, 165428-1-16 (2005)
39. To, C.W.S.: Bending and shear moduli of single-walled carbon nanotubes. Finite Elem. Anal. Des. **42**, 404–413 (2006)
40. Shen, L., Li, J.: Transversely isotropic elastic properties of single-walled carbon nanotubes. Phys. Rev. B **69**, 045414-1-10 (2004)
41. Krishnan, A., Dujardin, E., Ebbesen, T.W., Yianilos, P.N., Treacy, M.M.J.: Young's modulus of single-walled nanotubes. Phys. Rev. B **58**, 14013–14019 (1998)
42. Tombler, T.W., Chongwu, Z., Alxseyev, L., Jing, K., Hongjie, D., Lei, L., Jayanthi, C.S., Meijie, T., Shi-Yu, W.: Reversible electromechanical characteristics of carbon nanotubes under local-probe manipulation. Nature **405**, 769–772 (2000)
43. Hall, A.R., An, L., Liu, J., Vicci, L., Falvo, M.R., Superfine, R., Washburn, S.: Experimental measurement of single-wall carbon nanotube torsional properties. Phys. Rev. Lett. **96**, 256102-1-4 (2006)
44. Meo, M., Rossi, M.: Tensile failure prediction of single wall carbon nanotube. Eng. Fract. Mech. **73**, 2589–2599 (2006)
45. Lu, Q., Bhattacharya, B.: Fracture resistance of zigzag single walled carbon nanotubes. Nanotechnol. **17**, 1323–1332 (2006)
46. Xiao, J.R., Gama, B.A., Gillespie, J.W. Jr.: An analytical molecular structural mechanics model for the mechanical properties of carbon nanotubes. Int. J. Solids Struct. **42**, 3075–3092 (2005)
47. Yakobson, B.I., Brabec, C.J., Bernholc, J.: Structural mechanics of carbon nanotubes: from continuum elasticity to atomistic fracture. J. Comp.-Aided Mater. Des. **3**, 173–182 (1996)
48. Yu, M.F., Dyer, M.J., Chen, J.: Locked twist in multiwalled carbon-nanotube ribbons. Phys. Rev. B **64**, 241403-1-4 (2001)